Microsized particles of Aza222 polymer as a regenerable ultrahigh affinity sorbent for the removal of mercury from aqueous solutions

Accepted for publication in *Separation and Purification Technology* on June 7, 2013.

Published article DOI: 10.1016/j.seppur.2013.06.005

Julian S. Taurozzi[1], Mikhail Y. Redko[1,2], Karrie M. Manes[2*],

James E. Jackson[2], and Volodymyr V. Tarabara[1*]

[1] Department of Civil and Environmental Engineering, Michigan State University, East Lansing, MI 48824, USA

[2] Department of Chemistry, Michigan State University, East Lansing, MI 48824, USA

Keywords:

mercury, sorption, metal-cryptand complex, polymer sorbent, nitrogen complexant, regenerable sorbent

[*] Corresponding authors: tarabara@msu.edu (V. V. Tarabara) and maneskar@msu.edu (K. M. Manes)

Abstract

This paper reports the preparation and characterization of a microparticulate sorbent based on a novel *p*-xylylene-peraza[2.2.2]cryptand (Aza222) polymer that exhibits selectivity and high affinity for mercury cations [1-3]. The sorbent particles dispersed into an aqueous suspension were characterized in terms of surface morphology, size distribution, porosity, and surface charge. Based on measured adsorption isotherms, two possible mechanisms of adsorption by this novel sorbent are proposed: high affinity stoichiometric complexation of Hg^{2+} within the Aza222 cage, which proceeds until the stoichiometric capacity of the sorbent is saturated; then excess mercury removal by nonspecific physisorption onto the surface of the Aza222 polymer. The experimentally determined mercury loading capacity of the sorbent was in accord with stoichiometric calculations at both high (ppm) and low (ppb) concentrations, opening possibilities for the use of the polymer for mercury detection or other analytical applications. Desorption studies were carried out and the regenerability of the sorbent was demonstrated. The mercury capacity and selectivity of the sorbent in the presence of calcium ions compared favorably against corresponding properties of both a commercial ion exchange resin used for mercury removal and a related but non-macrocyclic polyamine-based polymer. Density functional (B3LYP) calculations using the 6-31G* basis set for light elements (C, H, Li, N, O) and the LANL2DZ effective core potential and basis set combination were used to compute the relative stability constants of the various metal-cryptand complexes. The agreement between theoretical and experimental Ks values, where known, was generally excellent, supporting the prediction of unknowns. Of particular relevance to the experimental work herein, the calculated

difference between log Ks for Hg^{2+} vs. Ca^{2+} ion binding in the hexamethylated peraza[2.2.2]cryptand is 23.0, indicating an overwhelming preference for binding mercury in this all-nitrogen complexant model for the ligand covalently imbedded in the Aza222 polymer sorbent.

Introduction

Mercury in its various forms - elemental, organic, or inorganic - is a toxic heavy metal that contaminates the environment via both natural processes and anthropogenic releases. In the United States, coal-fired power plants are the main source of human-caused mercury pollution accounting for more than 40% of the country's mercury emissions. As human populations increase and standards of living rise worldwide, rising demand for electricity will prompt increasing combustion of coal, with its attendant pollutant releases. Thus, development of systems for effective reduction of mercury pollution of air, soil, and water is a global priority.

The main physicochemical methods currently employed for mercury removal from water are chemical precipitation, ion exchange resins, and liquid phase sorption. Chemical precipitation involves the formation of insoluble compounds wherein mercury is either bound by sulfur-rich ligands or removed by coprecipitation with alum or ferric hydroxide. The advantage of chemical precipitation is that it can be used to treat feed waters with very high mercury concentrations; however, this method is not selective for mercury and the precipitates can be unstable over time or within certain pH windows, releasing mercury back into the environment [4-6]. Precipitation-based removal is also costly as it requires large quantities of co-precipitant to remove mercury to levels below the 2 ppb EPA standard for drinking water [4-8]. The other two currently used mercury removal methods - ion exchange and liquid phase sorption - can be more cost-effective, as ion exchange resins and sorbents are, in some cases, regenerable. Ion exchange resins bind mercury using terminal sulfur-containing groups and have higher loading capacities than carbon-

based sorbents [4, 9, 10]; however, their selectivity is low [11-14] because of the competition between mercury and much more abundant copper ions that not only successfully compete for binding with thiol groups, but also catalyze their oxidation with ambient molecular oxygen. Sorption-based methods employ a variety of sorbent materials such as activated carbon, which is widely used for the separation of mercury from liquid phases but is not selective for mercury [4, 9, 10]. Several other sorption-based strategies have been proposed encompassing a wide range of sorbent materials such as whey proteins, xanthate, keratin, polyelectrolytes, industrial waste wool and others [5, 11, 15-17]. Table 1 details the relative benefits and drawbacks of several of these mercury removal methods.

[Table 1]

A number of reports have described synthetic materials [23-27] with high affinity and/or selectivity for mercury cations. For sulfur-based sorbents, issues such as the long-term stability of the complexes vis-à-vis air oxidation were often not addressed. When sulfide-based materials are oxidized to sulfites or sulfates they are rendered ineffective at binding mercury, a problem avoided by nitrogen-based materials. Moreover, if insoluble HgS complexes are oxidized to $HgSO_4$, they become water-soluble and can be re-mobilized in effluent streams. Finally, mercury vs. copper competition, which can be important in nitrogen-based materials, was not addressed in previous papers. We have calculated [2] the effective Hg/Cu selectivity constant ($LogK^{eff,sel}_{Hg/Cu}$) for peraza[2.2.2]cryptand and compared it to the corresponding selectivity constants

of a variety of polyamine monomers. The obtained values suggest that peraza[2.2.2]cryptand outperforms other polyamines in its selectivity for mercury cations.

An ideal mercury-binding material would be air-stable, selective, easily regenerable, and have a high sorption capacity for mercury cations. In a search for such sorbents, we built on our synthesis of 1,4,7,10,13,16,21,24-octaazabicyclo[8.8.8]hexacosane by measuring the mercuric ion complexation stability constant of this polyamine complexant and by incorporating these potent complexing sites into a range of polymer materials (Fig. 1a) formed via various synthetic routes [2, 3].

[Figure 1]

In the present work, we report the preparation and characterization of a microparticulate sorbent based on *p*-xylylene-Aza222, a polymer with high affinity and selectivity for mercury cations [2, 3]. Scanning electron microscopy (SEM), laser diffraction, nitrogen adsorption, and electrophoretic mobility measurements were performed to assess surface morphology, size distribution, porosity and surface charge of the sorbent particles. Based on batch sorption reactor experiments to probe adsorption kinetics and adsorption isotherms, the mechanisms of mercury uptake by this novel sorbent were postulated and relevant adsorption parameters were determined. Desorption studies uncovered effective methods for sorbent regeneration. The

Aza222-based sorbent's performance was compared to those of a similarly prepared non-macrocyclic polyamine polymer and a commercially available ion exchange resin with and without environmentally relevant concentrations of calcium. Finally quantum chemical calculations were performed as a check on the measured stability constants of peraza[2.2.2]cryptand and several of its methylated and ether analogues with mercuric ion (log K_S = 28.5) and other possible competing metal ions.

Experimental

Materials. Mercury (II) chloride (Fluka, 99.5%), sodium iodide (Sigma-Aldrich, 99.5%), hydrochloric acid (EMD, 36% ACS grade), calcium nitrate tetrahydrate (Sigma-Aldrich, 99%) and sodium hydroxide (J. T. Baker pellets, 98.4%) were all used as received. Water used in all experiments was supplied by a commercial ultrapure water system (Lab Five, USFilter Corp., Hazel Park, MI) equipped with a terminal 0.2 μm capsule microfilter (PolyCap, Whatman Plc., Sanford, ME). The resistivity of water was greater than 16 MΩ·cm. All filters were used as received. The source material for the preparation of the sorbent particles was the microporous polymer Aza222 (Fig.1a). Cross-linked non-macrocyclic polyamines (polyethyleneimines) were also used for comparative purposes (Fig. 1b,c). Both syntheses are reported elsewhere [3]. The stability constant, K_L, of the Hg^{2+}-peraza[2.2.2]cryptand complex was measured to be $\log(K_L)$ = 28.5 ± 0.1 [2]. A commercially-available regenerable mercury adsorption resin, which is a thiol (mercapto) functionalized ion exchange resin, having high Hg^{2+} selectivity, was used as the comparative basis in the sorption experiments. This commercial resin is currently used in wastewater treatment.

Preparation of sorbent particles. Aza222, PEI1 and PEI2 particles were prepared by adding 2 g of the polymer source material to 100 mL of ultrapure water. The mixtures were sonicated for 30 h using a water bath sonicator (model 50T, VWR Aquasonic). The resulting opaque suspensions were then filtered through a polycarbonate hydrophilic track etch membrane filter (Isopore,

Millipore) with 0.22 μm nominal pore size using a pressurized stainless steel filtration cell (HP4750, Sterlitech Corp.) in the case of Aza222 or through a fritted glass filter (4 – 5.5 μm pore size) in the case of PEI1 and PEI2. Particles collected from the filter surface were allowed to dry for 24 h and then ground in a ceramic crucible to a finely dispersed state. To assess the resuspension capacity of particles, a portion of the finely ground dry powder was resuspended in water and sonicated for 1 min. Aqueous suspensions of all sorbent particles used were prepared by sonicating the fine powder in water for ~1 min.

SEM characterization of Aza222. SEM micrographs of the Aza222 particles were recorded using a Hitachi S-4700II field emission scanning electron microscope operated in an ultra high resolution mode. The SEM samples were prepared by distributing Aza222 particles over the surface of the carbon coated adhesive tape mounted on an aluminum stub. The samples were coated with pure osmium for 20 s at a current of 10 mA using an osmium plasma coater (NEOC-AT, Meiwa Shoji Co., Osaka, Japan).

Particle size distribution measurements. Particle size distribution and particle fractal dimension were measured using a light diffraction apparatus (Mastersizer 2000, Malvern Instruments, Worcestershire, UK). The suspension was introduced into the optical cell using a sample dispersion unit (Hydro 2000 SM, Malvern Instruments, Worcestershire, UK). For the description of particle charge measurements see the SI.

Nitrogen adsorption test. The total surface area of sorbent particles was determined by BET nitrogen physisorption (Micromeritics ASAP 2010, Micromeritics Instrument, Norcross, GA) at 78 K over the (0.0 to 0.2) range of the relative pressure, P/P_0. Surface area was calculated from the BET equation. Micropore volume was determined using the t-plot method and total pore volume was characterized as volume adsorbed at the maximum relative pressure of 0.99.

Determination of particle porosity. The porosity of the sorbent particles was calculated from the results of N_2 adsorption and settling experiments (see SI) using the assumption that both the aggregates and primary particles are spherical and that the primary particles are monodisperse.

Atomic absorption analysis. The aqueous concentration of mercury (II) in high concentration sorption and desorption (regeneration) studies was measured using Varian SpectrAA-200 flame atomic absorption (AA) spectrometer. Solutions of $HgCl_2$ in 1 mM aqueous HNO_3 containing 1, 3, 10, 30, 100, 300, and 1000 ppm Hg^{2+} were used as calibration standards. The lower detection limit was 3 mg(Hg)/L. Low mercury (II) concentration analysis (ppb) was carried out using cold vapor atomic absorption with a Cetac M6000A using high purity N_2 carrier gas. Commercially available solutions (Specpure plasma standard solutions, Alfa Aesar) containing 0.025, 0.100 and 0.500 ppb mercury (II) were used as calibration standards. The lower detection limit was 2 ppt, based on prior instrument calibration with NIST Certified Reference Material (mussel tissue) used in trace element analysis**.**

Aza222 adsorption kinetics measurements. Completely mixed batch reactor tests were carried out to determine the kinetics of mercury sorption by Aza222 sorbent particles. Kinetic adsorption experiments were done with a Hg^{2+} feed of 145.11 ± 1.07 ppm, a value chosen to be in excess of the theoretical Hg^{2+} capacity of the Aza222 in the batch yet still well within the specific sorption (flat) portion of the isotherm. Fixed amounts of $HgCl_2$ were added to 150 mL beakers each containing 120 mL of 0.1M NaI(aq), producing the highly stable HgI_4^{2-} complex, ensuring the presence of a predominant well-defined mercury species in solution and avoiding a complex mixture of mercuric chloride ions, hydrolyzed species and protons. Then, 20 mL of the solution from each beaker was separated for the determination of mercury content by AA. A fixed mass of dry Aza222 powder was added to the remaining 100 mL of feed solution. Immediately upon the addition of the sorbent, the suspension was sonicated to allow for the disaggregation of the sorbent particles. The batch reactors were then stirred continuously and 6 mL suspension samples were periodically withdrawn from each reactor. All samples were filtered through a polyvinylpyrrolidone-coated polycarbonate track-etched membrane filter (Whatman, Nuclepore) with 0.1 μm nominal pore size and the filtrates were analyzed by AA. Each experiment was performed in triplicate.

Adsorption kinetics modeling. Numerical modeling was employed to evaluate adsorption parameters by comparing model predictions and experimentally observed kinetics. The method employed for solving the homogeneous surface diffusion model (HSDM) as adopted from studies by Hand et al. on suspended sorbents in completely mixed batch reactors [28, 29]. In a completely mixed batch system with dissolved adsorbate and suspended particles of microporous

sorbent, the adsorbate is removed from the liquid phase as it partitions into and diffuses within the porous matrix of the sorbent particles. Solutions to the equations (1 - 4) describing this mass transfer process were developed under the following assumptions, which allowed for a simplification of the numerical algorithm: 1) pore diffusion is negligible with respect to surface diffusion, 2) surface diffusion can be described by Fick's law, 3) the porosity of sorbent particles has the same value for all particles and for all locations within each particle, 4) adsorbate mass flux within the liquid phase is driven by the difference between the liquid bulk concentration and the concentration at the sorbent's surface, 5) local adsorption equilibrium occurs at the solid-liquid interface, 6) the *local* equilibrium at the liquid-solid interface can be described by a Freundlich isotherm. The following equations express spatial and temporal variations in the concentration of the adsorbate in the adsorbed and liquid phases:

$$\frac{\partial q(r,t)}{\partial t} = \frac{D_s}{r^2}\frac{\partial}{\partial r}\left[r^2\frac{\partial q(r,t)}{\partial r}\right], \tag{1}$$

$$\frac{\partial C(t)}{\partial t} = -\frac{3\rho_a(1-\varepsilon)}{R^3\varepsilon}\frac{\partial}{\partial t}\int_0^R q(r,t)r^2 dr\,, \tag{2}$$

where $C(t)$ is the adsorbate concentration in the liquid phase at time t, $q(r,t)$ is the concentration of adsorbent in the solid phase at time *t* and radial coordinate *r*, D_s is the surface diffusion coefficient within the solid phase, ρ_a is the density of the adsorbent, ε is the volume fraction of the reactor occupied by the liquid phase, and R is the adsorbent particle radius (m).

The adsorbate mass flux towards the adsorbing solid is given by

$$\frac{\partial}{\partial t}\int_0^R q(r,t)r^2 dr = \frac{k_f R^2}{\rho_a \phi}\left[C(t) - C_s(t)\right] \quad (3)$$

and the local Freundlich equilibrium isotherm at the liquid-solid phase is given by

$$q(r = R, t) = KC_s t^{1/n}, \quad (4)$$

where K and n are the local Freundlich coefficients and $C_s(t)$ is the adsorbate concentration in the liquid phase at the solid-liquid interface. One boundary condition describes the initial solid phase adsorbate concentration: $q(0 \le r \le R, t = 0) = 0$, while another one reflects the spherical symmetry of the sorbent particle: $\frac{\partial q(r = 0, t \ge 0)}{\partial r} = 0$. To simplify the solution of the system of equations (1-4), the equations were non-dimensionalized (see SI). If it is assumed that at any time the liquid-phase mass transfer resistance is negligible in comparison with the solid-phase mass transfer (i. e. $C_s(t) = C(t)$), the model can be further simplified by eliminating (3) so that the only parameters to be specified are the Freundlich coefficient *n*, the surface diffusion coefficient D_s, the particle radius R, and the fraction of adsorbate remaining in the solution $\left(\frac{C_e}{C_0}\right)$.

Aza222 adsorption isotherm measurements. Adsorption isotherms encompassed a wide concentration range (2 to 2000 ppm) in order to obtain a comprehensive knowledge of the adsorption behavior of the material at both low and high concentrations and to gain a better

understanding of the adsorption mechanism(s) over a wide range of concentrations rather than emulating a specific feed type. Two sets of adsorption isotherm measurements were carried out. In the first set mercury was in excess with respect to the Aza222 sorbent while in the second set the sorbent was in excess with respect to mercury. In the first set, the feed samples were prepared by dissolving $HgCl_2$ in 70 mL of a 1 M NaI(aq) solution. Feed solution (20 mL) was separated for AA analysis. Five Teflon-capped stirred scintillation vials were filled with 10 mL of feed solution each and varying amounts of dry sorbent from ~ 6 to 100 mg were added to achieve the desired liquid phase concentration in each case. The suspensions were sonicated and then stirred for 24 h. One mL of each suspension was separated and added to a vial with 9 mL of ultrapure water. The diluted suspensions were filtered through a 0.1 μm polycarbonate filter and the filtrate was analyzed using AA. The amount of adsorbed mercury was calculated as the difference between the initial (feed) concentration and the measured equilibrium concentration of mercury in each vial. In the second set of experiments, the feed solutions were prepared as in the first set. Four Teflon-capped scintillation vials with different $HgCl_2$ feed concentrations were filled with approximately the same amount of the dry sorbent and stirred. The rest of the procedure was the same as in the experiments from the first set. The amount of mercury adsorbed by the particles (q_e) was expressed in mg/g as mass of adsorbate (mercury) per mass of sorbent (Aza222).

Aza222 sorbent regeneration study. A fixed amount of Aza222 particles were dispersed with sonication in a $HgCl_2$ solution prepared to stoichiometrically saturate the polymer's estimated sorption capacity (20% of its mass). Polymer dispersion was followed by 24 h of continuous

stirring to achieve equilibrium between liquid and adsorbed phases. The sorbent particles were filtered from the suspension using a 0.1 μm polycarbonate filter and then rinsed three times with ultrapure water to remove all non-sorbed mercury. After the third rinsing step, mercury levels in the rinsate were below the 3 ppm AA detection limit. The filtrate and Hg^{2+} feed solutions were both analyzed by AA to quantify the amount of mercury removed by adsorption onto the polymer from the feed solution. The filtered polymer was dried and weighed to account for possible mass losses during the filtration step. The polymer particles were subsequently redispersed in a saturated Na_2S solution to allow for the release of the polymer-bound mercury into the liquid phase. A saturated Na_2S solution was used in order to form the soluble complex Na_2HgS_2 and thus prevent the formation of an insoluble HgS precipitate. This mercury desorption study was conducted under continuous stirring for 24 h, after which the polymer was filtered, rinsed, and dried and the filtrate analyzed by AA using the same procedure as above. The regenerated polymer was digested using concentrated H_2O_2 and HNO_3 until the sorbent particles were completely dissolved. Digestion was accompanied by the emission of dark NO_2 gas characteristic of nitric acid digestion. The digest solution was analyzed by AA to quantify the amount of any residual sorbed mercury.

Mercury sorption in the presence of a competing divalent ion. To study the potential mitigation of the Aza222, PEI1 and PEI2 sorbents' Hg capacity due to the presence of competing divalent ions, a series of adsorption studies were conducted by adding $Ca(NO_3)_2$ salt to the $HgCl_2$ feed solution. Calcium nitrate was added at a 6:1 (Ca:Hg) molar ratio, where the mercury concentration was calculated to stoichiometrically saturate the Aza222 sorbent. Fixed amounts

of either Aza222, PEI1 or PEI2 particles were dispersed in the feed solution with the aid of sonication. The dispersion was followed by 24 h of continuous stirring to achieve adsorption equilibrium. The sorbent particles were filtered out from the suspension using a 0.1 μm polycarbonate filter. The filtrate and the feed solutions were analyzed by AA to quantify the amount of mercury removed from the feed solution by adsorption onto the polymer. Identical control experiments were performed for calcium-free solutions. The performance of the Aza222 sorbent was also compared with that of an existing commercial Hg sorbent on an equal mass loading basis.

Computational study of Hg^{2+} binding by cryptands. Quantum chemical modeling studies were carried out to ascertain the stability of Hg^{2+}-cryptand complexes, which may possibly explain the selectivity of the Aza222 sorbent for Hg^{2+}. Calculations were carried out using several oxa-, aza- and mixed oxa,aza-base representative cryptands with the Spartan '08 program [30] at the B3LYP level of theory using the 6-31G* basis set for all light elements (C, H, N, O). Third, fourth, and fifth-period metal cations were modeled using the LANL2DZ pseudopotential and basis set combination. Lowest energy conformations were obtained by optimization from various starting geometries and compared, where available, to known X-ray crystal structures.

Results and Discussion

Size and morphology of Aza222, PEI1 and PEI2 sorbent particles. Figure 2 illustrates particle size distributions of suspensions of i) as-synthesized Aza222 polymer (source material), ii) prepared Aza222 particles and iii) filtered and resuspended Aza222 particles. The SEM images of sorbent particles shown in Fig. 3 corroborate the results of light diffraction measurements and demonstrate that sorbent particles are porous aggregates ~10 μm in diameter. The aggregates were found to consist of primary particles (spherules) of ~1 μm in diameter. The aggregates were not fractal (see Supporting Information (SI), Fig. SI1) and had porosity of 0.38 ± 0.01 as calculated based on the results of N_2 adsorption measurements and particle settling experiments (see SI).

[Figure 2]

Nitrogen adsorption analysis of the dry sorbent powder demonstrated that the spherules had very low micropore volume and area (see SI, Table SI1), consistent with the results of the SEM imaging. The measured value (3.65 m²/g) of the BET surface area of Aza222 particles is close to the value predicted by assuming that 60% of the surface of 1 μm spherules, with a density of 1 g/mL, is available for N_2 adsorption (see SI, Table SI1). PEI1 and PEI2 sorbent particles had an average particle size of ~ 10 μm and a BET surface area of 3.08 m^2/g, comparable to that of the

Aza222.

[Figure 3]

Adsorption kinetics measurements and modeling. Mercury uptake kinetics for the Aza222 sorbent were measured to experimentally verify the theoretical value of the absolute adsorption capacity and to determine the time to equilibrium. The adsorption tests were carried out in a completely mixed batch reactor. Uptake kinetics were also predicted by the numerical homogeneous surface diffusion model [29] and the predicted kinetics were fit to the experimental data using the intraparticle diffusion coefficient D_s and the Freundlich coefficient n as fitting parameters. To simplify the interpretation of uptake kinetics data, experiment-to-experiment variations in the feed concentration of mercury and loading of the sorbent were factored out by expressing the results of three sorption experiments (Fig. 4) in terms of the normalized relative adsorption capacity R_n:

$$R_n(t) = \frac{R(t)}{R(0)} = \frac{C(t) - C_e}{C(0) - C_e}$$

where $C(0) = C(t = 0)$ is the initial feed concentration and $R(t)$ is the relative adsorption capacity given by the (normalized) difference between the liquid phase concentration $C(t)$ of mercury at a

given time and the theoretical liquid phase equilibrium concentration C_e achieved when the sorbent removal capacity is exhausted: $R(t) = \frac{C(t) - C_e}{C_e} \cdot 100\%$.

[Figure 4]

The absolute adsorption capacity of the material, expressed in terms of weight percent, was computed based on the amount of added sorbent, the mercury concentration in the feed, and the equilibrium mercury concentration. The measured C_e values yielded an absolute adsorption capacity for the suspended sorbent particles of 18.6 % wt/wt; that is, 1 g of Aza222 particles can capture 186 mg of dissolved mercury. The obtained experimental value is close to the theoretically estimated 20% wt/wt value, calculated based on the Aza222 molecular structure (see SI, Fig. SI2). Upon performing elemental analysis (CHN/O) of the Aza222 polymer, a molecular formula of $C_{48}H_{66}N_8Cl_{2.5} \cdot H_2O$ corresponds well to the experimental C, H, N and O content. This chemical formula suggests a structure with, on average, 2.5 secondary nitrogen atoms bearing a *p*-xylylene unit that is not bound to another cryptand cage. Based on the average molecular weight of this unit, the theoretical capacity of the Aza222 polymer would be 17.6% (see SI, Fig. SI3). The time to equilibrium was 6 h.

Upon equilibration, the value of the absolute adsorption capacity was found to be slightly higher than the theoretical 20% equilibrium value, which could be due to several factors:
(i) transfer losses during the weighing of Aza222 particles recovered from the filter cake,
(ii) small sample-to-sample differences in the amount of polymer removed from the batch reactor for AA analysis, or (iii) finite filtration time (up to 2 min), which was comparable to adsorption times for the first samples withdrawn from the batch reactor. Finite filtration time was viewed as a potential interference because as the suspension is filtered, the adsorption of mercury into the suspended particles and particles already deposited on the filter surface continues but now it is in the filter's pseudo plug flow reactor geometry, which is different from the stirred batch reactor geometry. The latter interference is also the likely explanation for the higher scatter of the data observed in earlier stages of the adsorption experiment (Fig. 5). To account for the additional mercury adsorption during filtration time (~ 1 min), a time offset of 1 min was added to each recorded batch adsorption time value.

Figure 4 shows the experimentally obtained kinetic data and the prediction of the model. The fitted surface diffusion coefficient in the solid phase, D_s, was found to be $9.0 \cdot 10^{-13}$ cm^2/s, which falls within the very wide reported range ($1 \cdot 10^{-9}$ to $8 \cdot 10^{-17}$) cm^2/s for solid phase diffusion coefficients for dissolved compounds in soils and sediments [29, 31-33]. The local Freundlich coefficient, n, was found to be 0.065 indicating favorable sorption ($n < 1$). Although the values of D_s and n were obtained with a coefficient of determination (r^2) value of 0.968, they should be viewed as coarse estimates in view of the assumptions of the homogeneous surface diffusion model [29]. The

finite width of the particle size distribution and the chemical complexation (rather than Freundlich physisorption) of mercury are considerations that might have affected the accuracy of the obtained values of D_s and n.

Adsorption isotherm measurements. A set of six independent adsorption experiments were conducted using the Aza222 sorbent, covering a wide range of mercury liquid phase equilibrium concentrations (Fig. 5).

[Figure 5]

The isotherm can be viewed as consisting of two segments. The first segment recorded for lower values of C_e (from 0 to ~1,200 ppm) is a high affinity isotherm indicative of adsorption so strong that no detectable mercury remains in the solution until the surface of the adsorbate approaches saturation. The plateau of the high affinity segment describes the complexation of Hg^{2+} within the Aza222 cage, confirming the theoretically estimated 20% wt/wt stoichiometric adsorption capacity. Such quantitative predictability of the Aza222's capacity to remove mercury could lead to the optimization of the sorbent's use and potentially be exploited in analytical applications (e.g. mercury detection).

The second segment recorded for higher values of feed concentrations (>1,200 ppm) corresponds to an adsorbent loading exceeding 20% and becoming higher for higher values of the equilibrium liquid phase concentration, C_e. This segment of the overall isotherm describes non-specific physisorption, which occurs after cage complexation sites are saturated and may be explained by strong ion pairing between the Hg^{2+} -cryptand binding sites and excess HgI_4^{2-} ions[34]. The environmental significance of this result is in the ability of the sorbent to operate under high mercury feed loadings and mitigate potential spikes in feed mercury concentrations. It should be noted, however, that the equilibrium Hg^{2+} concentration threshold, beyond which the non-specific physisorption occurs (1,200 ppm), is much higher than mercury concentrations typical for environmental samples.

Regeneration study. Exploratory studies (data not shown) confirmed that the sorbent could be regenerated by percolation of a saturated Na_2S solution through a column packed with sorbent. The present study was performed under batch conditions to obtain a comprehensive understanding of the polymer's regeneration behavior. Results obtained from the analysis of the feed and filtrate solutions for both aqueous phase adsorption and Na_2S regeneration steps showed that upon regeneration using saturated Na_2S aqueous solution, the polymer was able to release 85.5 % of the initially captured mercury. Thus, the environmental application of the developed sorbent can follow the sorption – separation – regeneration sequence typical of regenerable sorbents, such as powdered activated carbon, but with much higher affinity and selectivity for mercury compounds.

Mercury sorption using non-cryptand containing sorbents. To ascertain whether the presence of the cryptand was needed to effectively bind mercury, a set of two non-cryptand polyamine sorbents were synthesized: PEI1 and PEI2 (Fig. 1). The exposure to a high concentration (561 ppm) of Hg^{2+} resulted in PEI1 sorbing 1650 mg(Hg^{2+})/g(PEI1) and PEI2 sorbing 77 mg(Hg^{2+})/g(PEI2) (Fig. 6).

[Figure 6]

The capacity of the PEI1 was much higher than that of the Aza222 polymer under these conditions. One possible explanation for this result is that, on average, the PEI polymers may have more protonated amine sites since there are more secondary versus tertiary nitrogen atoms. Therefore the very high capacity of PEI1 may be due to ion-pairing between protonated amine sites and HgI_4^{2-} ions from the feed (physisorption) rather than Hg-N bond making (chemisorption).

Mercury sorption in the presence of a competing divalent ion: Comparison with a commercially available material. A commercial resin with similar characteristics to that of the developed Aza222 sorbent, i.e., high capacity, regenerability and selectivity with respect to calcium, was selected as an appropriate comparative control. Calcium is an environmentally

relevant interference ion since it is found in high quantities (~ 350 ppm) in coal-fired scrubber waste effluents [35], Aza222 did not sorb Ca^{+2} in detectable quantities and its capacity for Hg^{2+} was found to be higher than that of the commercial resin in the absence, and, to an even larger extent, in the presence of calcium ions (Fig. 7). Further optimization of Aza222 processing strategies may yield even higher mercury recoveries.

[Figure 7]

PEI1 and PEI2 were also analyzed for their Hg^{2+} selectivity in the presence of calcium in order to compare their performance to that of the Aza222 polymer under similar conditions. As seen on Fig. 8, the presence of Ca^{2+} ions severely hinders Hg^{2+} binding for both PEI1 and PEI2, which falls dramatically to 10.4% and 4.5% of the initial Hg content in PEI1 and PEI2, respectively. While PEI1 has the ability to bind much higher levels of Hg^{2+} than Aza222, its practical use is not feasible given its high affinity for Ca^{2+} ions and their abundance in waste effluents. One obvious possible mechanism by which Hg^{2+} uptake by the PEI polymers might be eroded is protonation of the amine sites by carbonic acid, formed when carbon dioxide dissolves in aqueous solutions.

$$\text{Resin}\ (s) + H_2O\ (l) + CO_2\ (aq) + Ca^{2+}\ (aq) \rightarrow \text{Resin*}2H^+\ (s) + CaCO_3(s)$$

As the nitrogen sites are protonated their ability to bind Hg^{2+} ions would be diminished. However, experiments measuring particle charge (see SI, Fig. SI4) in the absence and presence of CO_2 for both PEI and Aza222 polymer showed no evidence for this process.

Computational study of Hg^{2+}-cryptand complexes. A series of Density Functional Theory (DFT) calculations were run to probe the binding energetics of ligands in the [2.2.2]cryptand family with respect to the metal cations K^+, Hg^{2+}, and Cd^{2+} in aqueous solution. The Spartan '08 software package was used, running on several Macintosh and Linux-based PCs. Multiple duplicate calculations were run to ensure that the software versions on the respective platforms obtained identical results. The popular B3LYP functional with the 6-31G* basis set (for C, H, Li, N, and O) and LANL2DZ (for K, Ca, Cd, and Hg) basis set/pseudopotential combination were used in light of previous successes of these tools in investigations of ion binding in cryptands and closely related systems [36, 37].

[Figure 8]

Five metal cations (Li^+, K^+, Ca^{2+}, Hg^{2+} and Cd^{2+}), five complexants (**I** to **VI**; see Fig. 8), and three complexation geometries (see Fig. 9) were considered for this series of cryptate structures. The three conformations herein are termed staggered (ST), gauche (GA), and twist (TW), in order of decreasing cavity (and hence bound ion) size. The ST form is optimal for larger guest

ions such as K^+, while contraction to the TW geometry is required to bind small ions like lithium, as illustrated in Fig. 9.

[Figure 9]

Energetics. Before examining the structural and energetic characteristics of the metal cryptate complexes in detail, a look at the effects of the structural variations among the free ligands is in order. Direct guidance from X-ray structures is only available [38, 39] for free ligands **I**-**III**, but both **I** and **III** adopt the same conformation, as shown in Fig. 10. For the mixed N/O ligands **IV**-**VI**, a reasonable interpolation, supported by exploratory conformational analyses, was that these compounds too would adopt that same all-trans bridge geometry.

[Figure 10]

Replacement of ether oxygen moieties with secondary amine sites (i.e. **I** → **II**) has little effect on the strain energies of the free complexants or their complexes. However, replacement of ether oxygens with methylated nitrogens to form tertiary amine sites (i.e. **I** → **III** via **IV**-**VI**) evidently introduces substantial added strain due to the methyl groups' steric demands, which decrease the bridges' conformational flexibility. These variations in strain can best be appreciated via the following isodesmic reactions, in which the dimethylamine, dimethyl ether, and trimethylamine

components are considered to be “strainless” partners. Notably, the overall strain energy increase upon replacement of all ether oxygens with methylated nitrogens (i.e. **I → III**) is more than 30 kcal/mol.

I	+	$6(CH_3)_2NH$	→	**II**	+	$6(CH_3)_2O$	ΔE = -1.0 kcal/mol
I	+	$(CH_3)_3N$	→	**IV**	+	$(CH_3)_2O$	ΔE = +5.2 kcal/mol
IV	+	$(CH_3)_3N$	→	**V**	+	$(CH_3)_2O$	ΔE = +5.6 kcal/mol
V	+	$2(CH_3)_3N$	→	**VI**	+	$2(CH_3)_2O$	ΔE = +11.0 kcal/mol
VI	+	$2(CH_3)_3N$	→	**III**	+	$2(CH_3)_2O$	ΔE = +10.6 kcal/mol
I	+	$6(CH_3)_3N$	→	**III**	+	$6(CH_3)_2O$	ΔE = +32.4 kcal/mol

Complexes and their Structures: In 1978 Lehn and Montavon reported stability constants, log K_s for a large collection of metal cations binding to six cryptands including **I** and **IV-VI** [40]. The focus in that paper was on titrimetric determination of the binding strength and especially the complexants’ selectivity for or against metals of concern as toxic elements, including mercury and cadmium. For the metals of concern herein, an excerpt of the table published by Lehn and Montavon K_s is presented below.

[Table 2]

Though not discussed in the Lehn and Montavon paper, the sequential replacement of the oxygens in **I** with N-CH_3 moieties dramatically and monotonically improved on the already impressive affinity of this cryptand framework for mercury in particular. It seemed natural to take the next step and explore the ability of all-nitrogen cryptands. Recent work in the Jackson and Dye research groups to build room-temperature stable alkalide and electride complexes based on such all-nitrogen cryptands had led to an improved and scalable synthesis of **II** [1]. Thus it also became feasible to build and incorporate such frameworks into substances intended to serve as high affinity, reversible and reusable mercury scrubbing agents.

Rational design of synthetically challenging systems calls for a self-consistent and inexpensive strategy for predicting which systems should show most promise before investing in the molecule building process. In this case, for design of complexant systems, values of binding constants like those reported by Lehn and Montavon are the desired items. By computing energetics, and therefore equilibrium constants, for ion transfer among the well characterized ligands of Lehn and Montavon, our hope was to extrapolate to new candidate compounds and to focus on structural features of greatest value. However, as noted above, multiple conformational possibilities exist not only for uncomplexed ligands, but also for cryptate complexes.

Stability Constant Evaluations. Table 3 collects the DFT-computed energies of the lowest energy conformations (labeled) of the five free ligands and the complexes computationally

analyzed in this work. Each entry shows

(a) the conformational label;

(b) the B3LYP/6-31G* total energy (Hartrees) of the fully geometry optimized complex;

(c) the calculated energy change (kcal/mol) for the following ion transfer;

$$M^{n+}@\mathbf{I} + L(\text{empty}) \rightarrow M^{n+}@L + \mathbf{I}(\text{empty})$$

(d) the calculated log Ks value computed from this interaction; and

(e) the corresponding experimental value, where it is known.

[Table 3]

The anchor reference points for these calculations are the very well characterized log Ks values for the original [2.2.2]cryptand, **I**. With this simple strategy, with no fitting parameters, the match to the observed log Ks values, where known, is remarkably good, and the projected numbers therefore suggest that the peraza ligands should bind mercury extremely strongly.

Conclusions

Microparticulate sorbent based on the recently synthesized p-xylylene-Aza222 (Aza222) polymer is shown to exhibit selectivity and extremely high affinity for mercury cations with a measured log K value of 28.5 ± 0.1. Mechanisms of Hg^{2+} adsorption by this novel material are elucidated to include 1) high affinity stoichiometric complexation of Hg^{2+} within the Aza222 cage proceeding until the stoichiometric capacity of the sorbent is saturated, and 2) removal of excess Hg^{2+} by nonspecific physisorption onto the surface of the Aza222 polymer. Importantly, the loading capacity of the Aza222 sorbent is predicted from the stoichiometry of Hg^{2+} complexation by p-xylylene-Aza222 opening opportunities to extend the use of the polymer to Hg^{2+} detection or other analytical applications. The Hg^{2+} capacity and selectivity (in the presence of Ca^{2+} as competing adsorbate) of the Aza222-based sorbent is compared to that of a commercial sulfur-based ion exchange resin, selected to serve as the comparative basis due to its combination of high sorption capacity, regenerability, and selectivity with respect to Ca^{2+}. The novel polymeric sorbent surpasses the tested resin in the aforementioned mercury sorption properties. The Aza222-based sorbent also compares favorably with two similarly cross-linked but non-macrocyclic polyethyleneimine-based polymers. While one of these polymers had a higher capacity for Hg^{2+} in ultrapure water, its Hg^{2+} binding was severely hindered in the presence of Ca^{2+}. Such hidrance was not observed for Aza222-based sorbent underscoring the advantage of the uniquely high mercury affinity of this material. Indeed, the difference between log Ks for Hg^{2+} vs. Ca^{2+} ion binding was computed in density functional calculations to be 23.0,

indicating an overwhelming preference for mercury in this all-nitrogen complexant model for the ligand covalently imbedded in the Aza222 polymer sorbent. Finally, desorption studies demonstrated that the novel sorbent is regenerable.

Acknowledgements

This material is based upon work supported in part by the National Science Foundation under research grants BES-604368 and OISE-0530174 and in part by the MSU College of Engineering. JST acknowledges support by Nordberg and McCowan fellowships.

Supporting Information

The supporting information file contains additional data on the comparison of currently practiced mercury removal methods and characterization of sorbent properties, such as porosity, fractal dimension, adsorption capacity, surface area, and surface charge.

Figure captions

Figure 1: Molecular structure of (**a**) poly[peraza[2.2.2]cryptand/α, α'-dichloro-*p*-xylene] (Aza222) and (**b** and **c**) poly[polyethyleneimine/α, α'-dichloro-*p*-xylene].

Figure 2: Particle size distribution of i) as-synthesized Aza222 polymer (source material) dispersed in water ii) Aza222 particles, and iii) Aza222 particles filtered and then resuspended in water.

Figure 3: SEM micrographs demonstrating that sorbent particles are aggregates composed of fused spherules ~ 1 μm in diameter with no observable microporosity (inset).

Figure 4: Aza222 suspensions relative adsorption capacity as measured from kinetic experiments (diamonds) and as obtained from the numerical model fitting procedure (line).

Figure 5: Adsorption isotherms for the mercury uptake by Aza222 sorbent particles. Initial mercury concentration is 145.11 ± 1.07 ppm.

Figure 6: Hg^{2+} uptake by PEI-based and Aza22 in the absence of competing Ca^{2+} ions and in the presence of a six-fold excess of Ca^{2+}.

Figure 7: Hg^{2+} and Ca^{2+} sorption capacities of Aza222 and the commercial resin. For each data set, the first column represents the amount of adsorbed Hg^{2+} in absence of Ca^{2+}, the second column represents the amount of adsorbed Hg^{2+} in the presence of Ca^{2+}, and the third column represents the amount of adsorbed Ca^{2+} in the presence of Hg^{2+}. Error bars correspond to a 95% confidence interval.

Figure 8: Complexants examined and compared via DFT calculations.

Figure 9: Complexes presented in end-on and side views highlighting conformational variations that accommodate encapsulated ions of various sizes. The displayed structures correspond to known X-ray structures for these complexes, and indeed were the lowest energy conformations computed in each case. Left: Compound **I**, the [2.2.2]cryptand, enclosing a relatively large K+ ion (radius = 1.33 Å), and therefore adopting the ST conformation, as described above [1]. Center: Ligand **II** in the GA conformation, enclosing the smaller Cd^{2+} ion (radius = 1.03) [1]. Right: Again **I**, but here adopting the TW conformation, to best coordinate its very small Li^{+} guest ion (radius = 0.78) [1].

Figure 10: Free ligand structures **I**, **II**, and **III**, showing the conformational preferences found by X-ray crystallography. Note the conformational similarities of the original [2.2.2]cryptand **I** and **III**, despite the addition of six methyl groups in the latter framework. Interestingly, the unmethylated peraza[2.2.2]cryptand **II** adopts a crystal conformation that orients five of its six N-H sites inward.

a. Although the Cd^{2+} ion has not been studied at MSU, carefully purified samples of peraza[2.2.2]ligand **II** were sent to Prof. Nathaniel Finney, then at the University of Zurich in Switzerland, where his research group added a fluorescent side chain to create a fluorescent marker for heavy metal contaminations. This material's greatest success (as yet still unpublished) was with Cd^{2+} sensing.

b. *Ks* determined in this work.

Table captions

Table 1: Summary of mercury removal methods

Notes:
N: Non selective, non regenerable, not studied or not applicable. Notion used if absorption of Cu^{2+} was not studied, even if it was studied for other metal cations.
Y: Selective or regenerable
STC: Sodium thiocarbamate, STDC: Sodium dimethyldithiocarbamete, $BDETH_2$: 1,3-benzenediamidoethanethiol, TMT: 2,4,6-trimercaptotiazine, trisodium salt nonahydrate, $PyDETH_2$: pyridine-2,6-diamidoethanethiol

* No quantitative information on selectivity is provided. KI used for the resin regeneration, which indicates weaker binding in comparison with Aza222-based resin.

Table 2: Calculated log K_S values for ligands **I**, **IV**, **V** and **VI** with various metal cations.

Table 3: B3LYP/6-31G* (C,H,Li,N,O) + LANL2DZ (K,Ca,Cd,Hg) energies and derived ion transfer energies (kcal/mol) along with a comparative presentation of calculated and experimental stability constants [40].

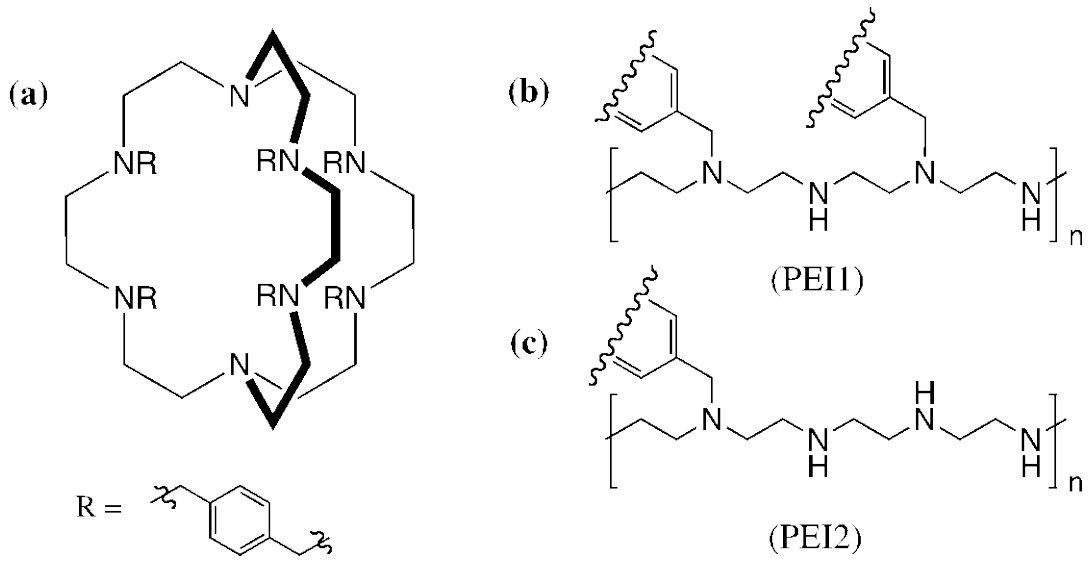

Figure 1

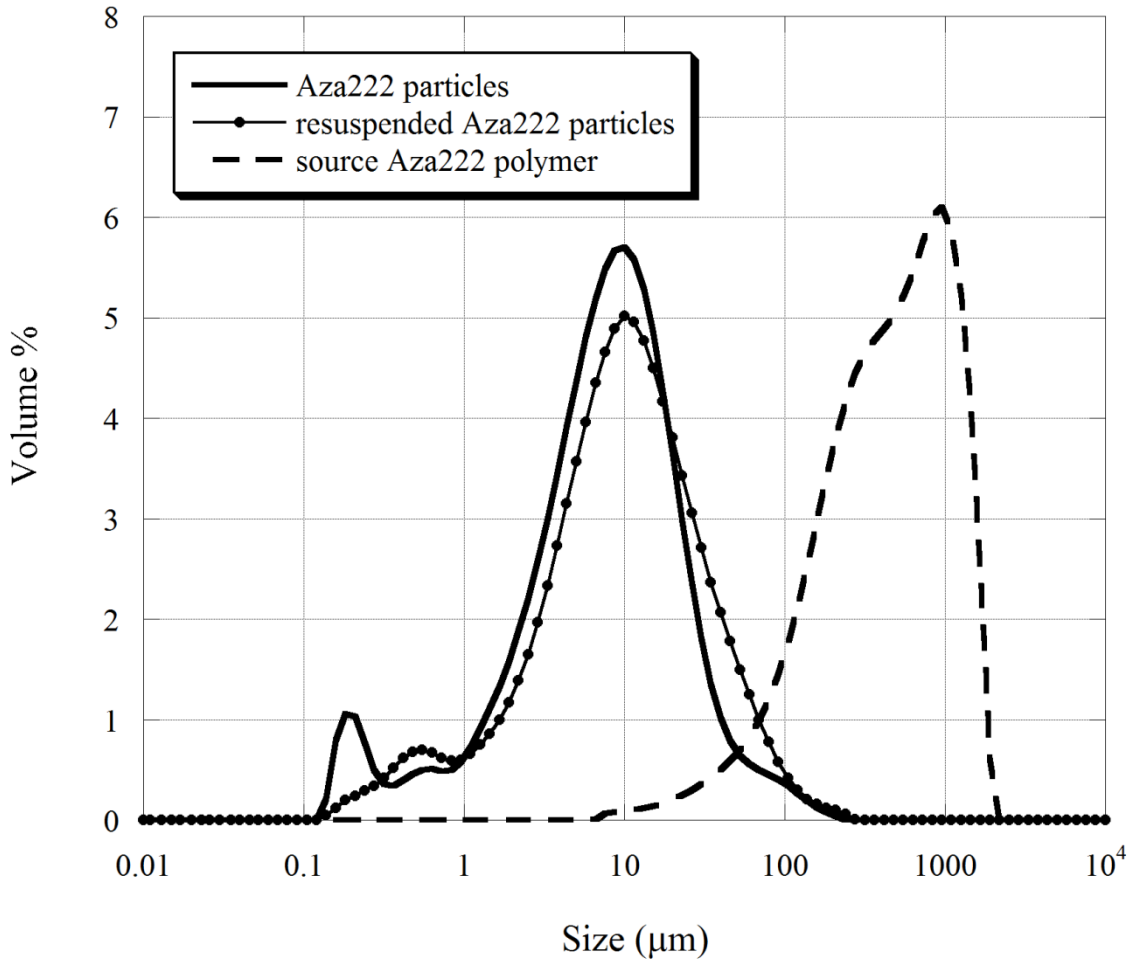

Figure 2

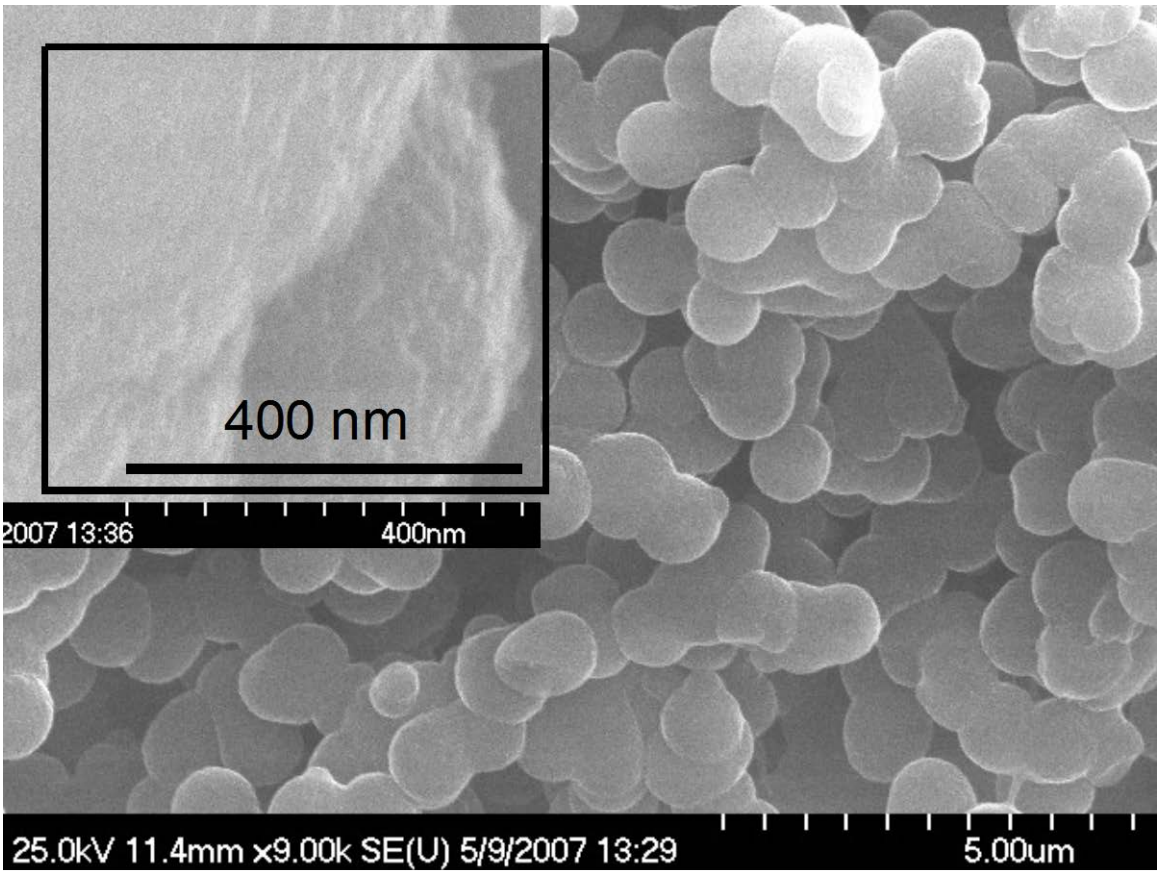

Figure 3

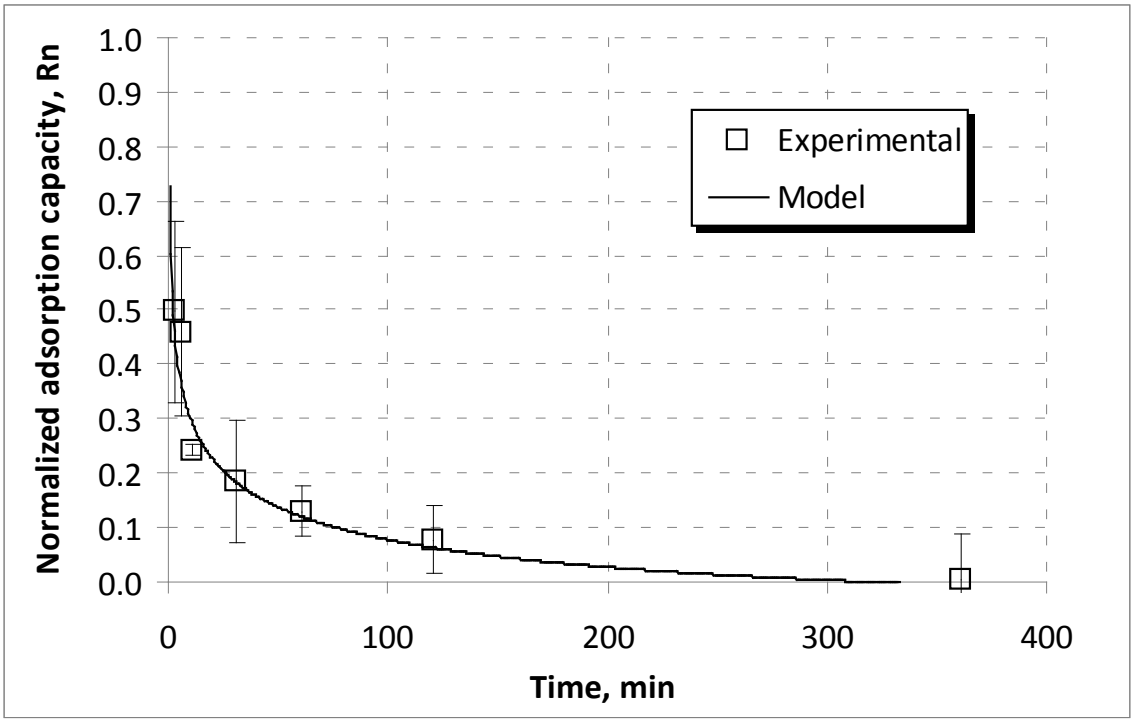

Figure 4

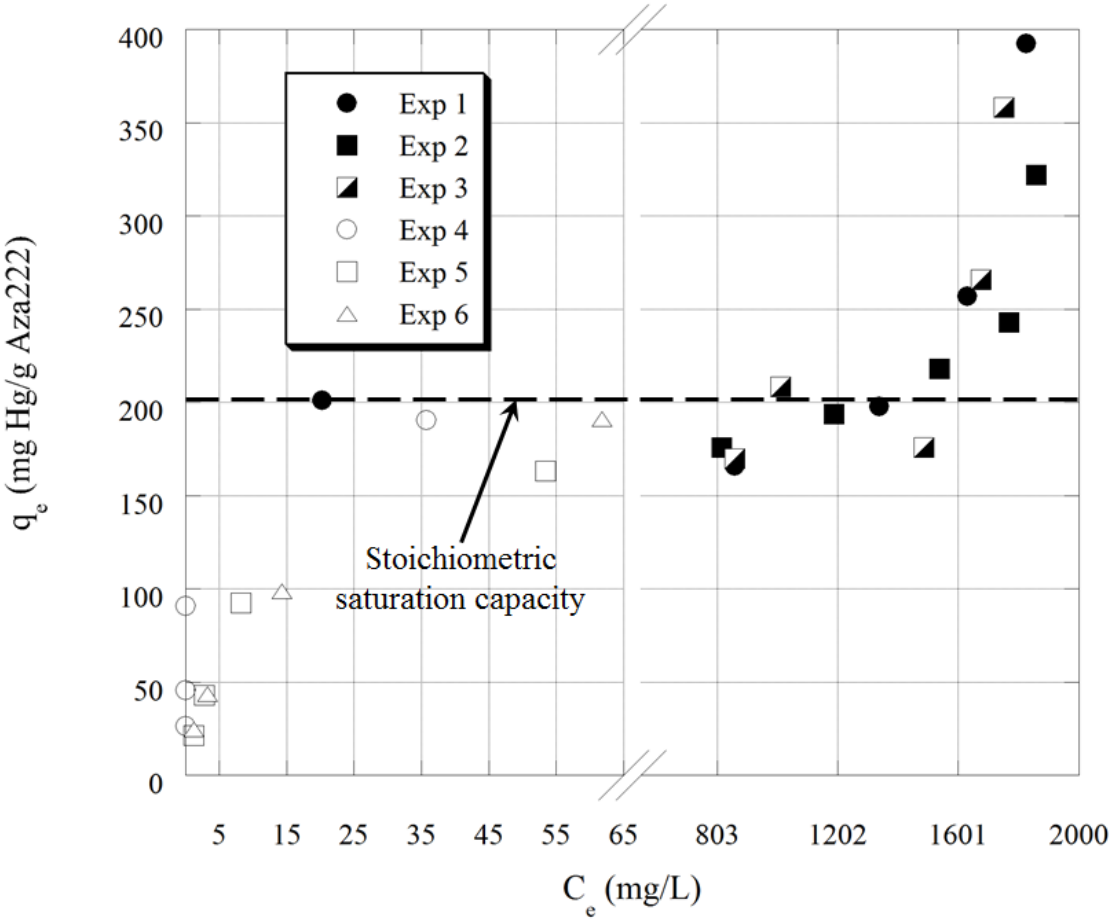

Figure 5

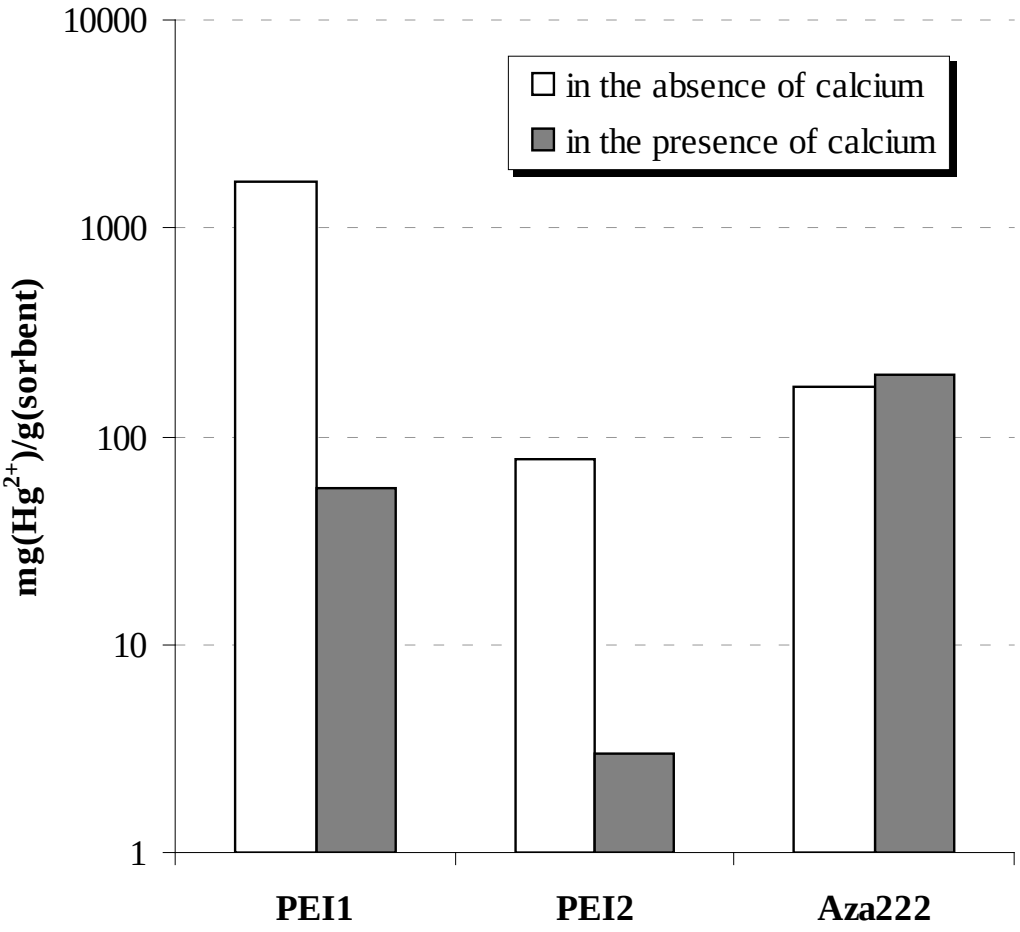

Figure 6

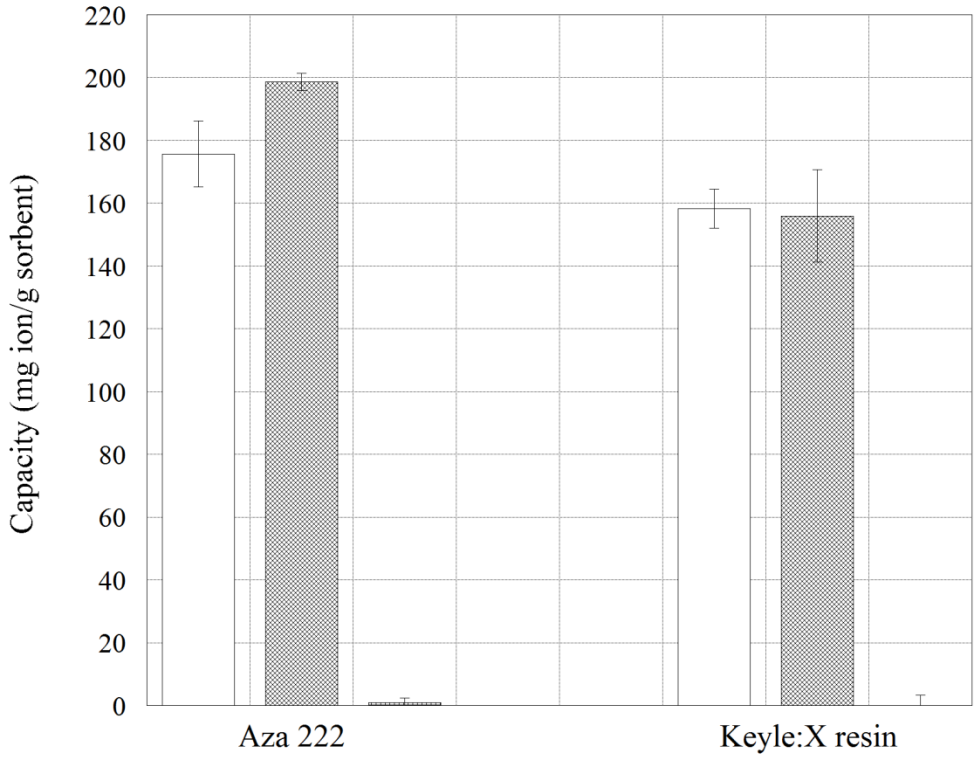

Figure 7

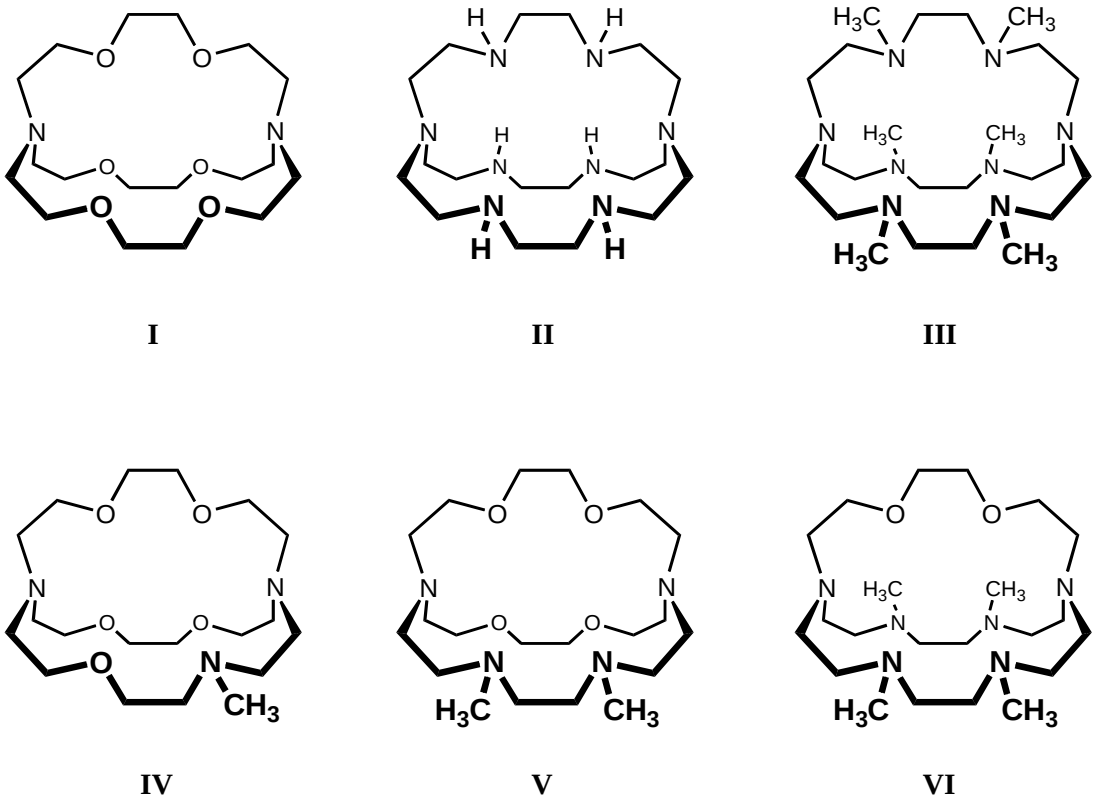

Figure 8

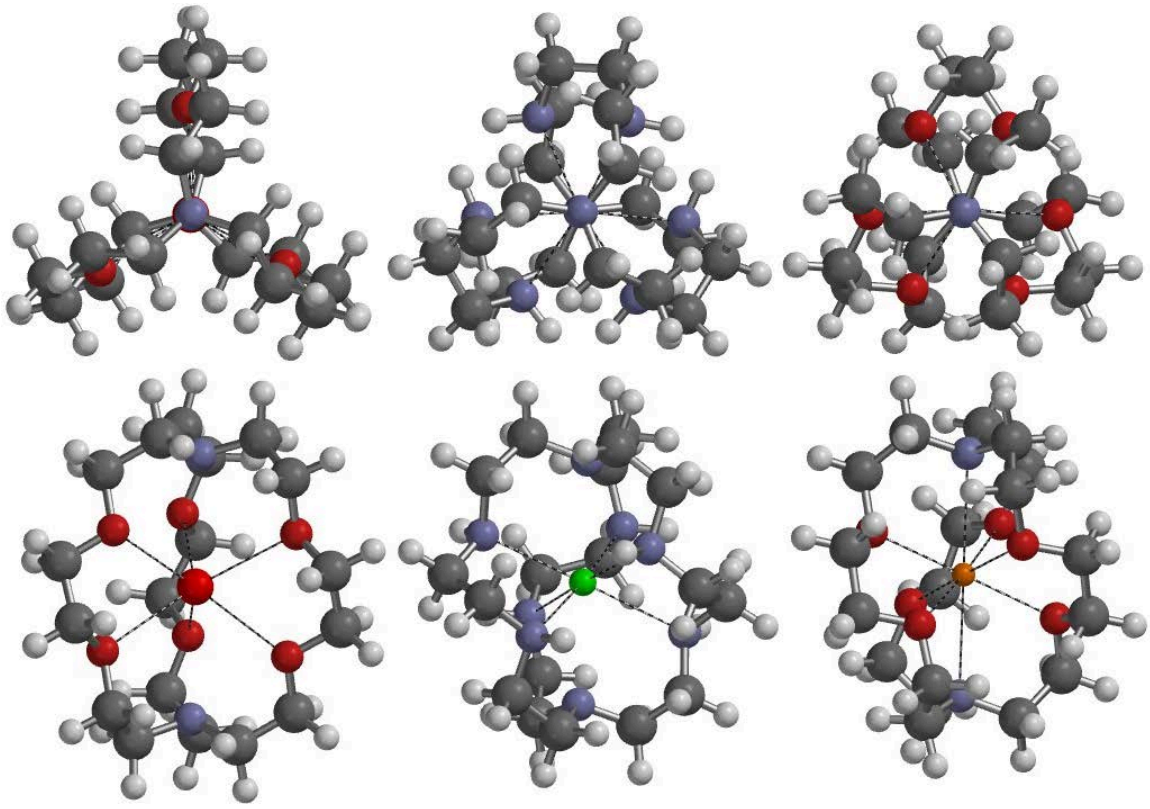

Figure 9

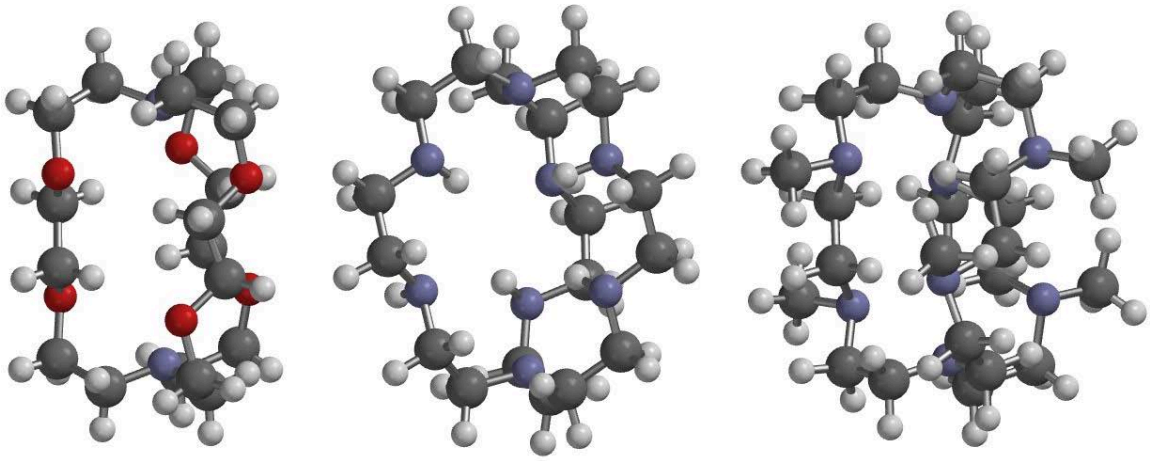

Figure 10

Method	Materials	Selectivity	Regenerability	References
Sorption	Whey, xanthate, keratin, polyelectrolyes, industrial waste wool, activated and sulfur impregnated carbon, chelating polymer	**N**	**N**	[1-6]
	Tannery hair, chelating fibers, starch xanthate and cationic polymer, triazole polymer, polymer-supported thiazacrowns, thiourea-glutaraldehyde chitozan resin*	**N**	**Y**	[2, 7-13]
Ion Exchange	Rohm and Haas (TMR), Srafion Anion exchange, shredded rubber, reduced MoS_2 and WS_2	**N**	**Y**	[2, 14, 15]
Precipitation	SDTC, STC, TMT, $PyDETH_2$, $BDETH_2$	**N**	**N**	[6, 10-12]
Microbial demercurization	Details in the reference	**N**	**N**	[16]
Functionalized porous matrices	Thiol functionalized membrane, thiol functionalized mesoporous silica substrate	**N**	**Y**	[17, 18]

Table 1

Table 2

Metal Cation	Ionic Radius (Å)	Log *Ks* with ligands [40]			
		I	**IV**	**V**	**VI**
Li^{+}	0.78	<2.0	1.5	2.4	–
K^{+}	1.33	5.4	4.2	2.7	1.7
Ca^{2+}	1.06	4.4	4.6	4.3	1.5
Cd^{2+}	1.03	7.1	9.7	12.0	10.7
Hg^{2+}	1.12	18.2	21.7	24.9	26.1

	Cryptand[2.2.2] species					
	I	**IV**	**V**	**VI**	**III**	**II**
(ligand sites)	O_6	$O_5(MNMe)$	$O_4(NMe)_2$	$O_2(NMe)_4$	$(NMe)_6$	$(NH)_6$
Empty	-1268.31608	-1287.75710	-1307.19754	-1346.07868	-1384.96035	-1149.14456
Li^+	TW	TW	GA	ST	ST	ST
Total E (H)	-1275.79994	-1295.24082	-1314.67631	-1353.54508	-1392.41827	-1156.61015
ΔE(kcal/mol)	[0]	0.1	3.2	11.0	16.3	11.5
Ks(calc)	[<2.0]	1.9	-0.3	-6.0	-9.9	-6.4
Ks(expt)	***<2.0***	***1.5***	***2.4***			
K^+	ST	ST	ST	ST	ST	ST
Total E (H)	-1296.42631	-1315.86461	-1335.30221	-1374.17841	-1413.05341	-1177.22587
ΔE(kcal/mol)	[0]	1.7	3.5	6.6	10.8	18.1
Ks(calc)	[5.4]	4.1	2.8	0.6	-2.5	-7.9
Ks(expt)	***5.4***	***4.2***	***2.7***	***1.7***		
Ca^{2+}	TW	TW	GA	GA	GA	GA
Total E (H)	-1304.62483	-1324.07014	-1343.51387	-1382.38675	-1421.25183	-1185.45727
ΔE(kcal/mol)	[0]	-2.7	-4.8	0.4	10.8	-2.5
Ks(calc)	[4.4]	6.4	7.9	4.1	-3.5	6.2
Ks(expt)	***4.4***	***4.6***	***4.3***	***1.5***		
Cd^{2+} [a]	TW	TW	GA	GA	GA	GA
Total E (H)	-1316.00657	-1335.45288	-1354.89937	-1393.77304	-1432.63436	-1196.84895
ΔE(kcal/mol)	[0]	-3.3	-7.1	-2.4	10.3	-8.7
Ks(calc)	[7.1]	9.5	12.3	8.9	-0.5	13.5
Ks(expt)	***7.1***	***9.7***	***12.0***	***10.7***		
Hg^{2+}	TW	GA	GA	GA	GA	GA
Total E (H)	-1310.638576	-1330.08879	-1349.53877	-1388.41969	-1427.28575	-1191.48910
ΔE(kcal/mol)	[0]	-5.8	-11.8	-11.6	-1.8	-13.8
Ks(calc)	[18.2]	22.4	26.8	26.7	19.5	28.3
Ks(expt)	***18.2***	***21.7***	***24.9***	***26.1***		***28.5*** [b]

References

[1] M.Y. Redko, R. Huang, J.L. Dye, J.E. Jackson, One-pot synthesis of 1,4,7,10,13,16,21,24-octaazabicyclo[8.8.8]hexacosane - The peraza analogue of [2.2.2]cryptand, Synthesis 5(2006) 759-761.

[2] M.Y. Redko, J.S. Taurozzi, K.M. Manes, J.E. Jackson, V.V. Tarabara, Development of Aza222-based polymers, colloidal sorbents, and membranes for the removal of mercury from aqueous solutions, in: 233rd ACS Meeting, Chicago , IL, 2007, pp. SUST 154.

[3] M.Y. Redko, J.S. Taurozzi, K.M. Manes, J.E. Jackson, V.V. Tarabara, Synthesis and characterization of Aza222-based polymers for the removal of mercury from aqueous solutions. In preparation.

[4] EPA, United States Environmental Protection Agency. About Mercury: Mercury basic information. http://www.epa.gov/hg/about.htm

[5] M.K. Zaman, Mercury removal from water, in: D.A. Atwood (Ed.) Recent Developments In Mercury Science: Structure and Bonding Series 120, Springer-Verlag, Berlin, Germany, 2006, pp. 163-182.

[6] M.M. Matlock, K.R. Henke, D.A. Atwood, Effectiveness of commercial reagents for heavy metal removal from water with new insights for future chelate designs, J. Hazard. Mater., 92 (2002) 129-142.

[7] M.M. Matlock, B.S. Howerton, D.A. Atwood, Irreversible precipitation of mercury and lead, J. Hazard. Mater., 84 (2001) 73-82.

[8] M.M. Matlock, B.S. Howerton, K.R. Henke, D.A. Atwood, A pyridine-thiol ligand with multiple bonding sites for heavy metal precipitation, J. Hazard. Mater., 82 (2001) 55-63.

[9] F. Tassel, J. Rubio, M. Misra, B.C. Jena, Removal of mercury from gold cyanide solution by dissolved air flotation, Miner. Eng., 10 (1997) 803-811.

[10] A.E. Gash, A.L. Spain, L.M. Dysleski, C.J. Flaschenriem, A. Kalaveshi, P.K. Dorhout, S.H. Strauss, Efficient recovery of elemental mercury from Hg2+-contaminated aqueous media using redox-recyclable ion-exchange materials, Environ. Sci. Technol., 32 (1998) 1007-1012.

[11] D.L. Michelsen, J.A. Gideon, G.P. Griffith, J.E. Pace, H.L. Kutat, Removal of soluble mercury from waste water by complexing techniques, in, NTIS, 1975.

[12] C. Calmon, H. Gold, Ion Exchange for Pollution Control, CRC Press, West Palm Beach, FL, 1979.

[13] W. Hollerman, L. Holland, D. Ila, J. Hensley, G. Southworth, T. Klasson, P. Taylor, J. Johnston, R. Turner, Results from the low level mercury sorbent test at the Oak Ridge Y-12 Plant in Tennessee, J. Hazard. Mater., 68 (1999) 193-203.

[14] M.C. Dujardin, C. Cazé, I. Vroman, Ion-exchange resins bearing thiol groups to remove mercury. Part 1: synthesis and use of polymers prepared from thioester supported resin, React. Funct. Polym., 43 (2000) 123-132.

[15] E.R. Russell, Removal of mercury from aqueous solutions by shredded rubber, in, 1975.

[16] L.P. Buckley, S. Vijayan, G.J. McConeghy, S.R. Maves, J.F. Martin, Removal of soluble toxic metals from water, in, At. Energy Can. Ltd., 1990.

[17] J.P. Tratnyek, Waste wool as a scavenger for mercury pollution in waters, in, 1972.

[18] R.D. Vidic, Adsorption of elemental mercury by virgin and impregnated activated carbon, in: A.K. SenGupta (Ed.) Environmental Separation of Heavy Metals, CRC Press, Boca Raton, FL, 2002, pp. 15-44.

[19] C.Q. Liu, Y.Q. Huang, N. Naismith, Novel polymeric chelating fibers for selective removal of mercury and cesium from water, Environ. Sci. Technol., 37 (2003) 4261-4268.

[20] J. Leonhäuser, M. Röhricht, I. Wagner-Döbler, W.D. Deckwer, Reaction engineering aspects of microbial mercury removal, Eng. Life Sci., 6 (2006) 139-148.

[21] J. Liu, X. Feng, G.E. Fryxell, L.Q. Wang, A.Y. Kim, M. Gong, Hybrid mesoporous materials with functionalized monolayers, Adv. Mater., 10 (1998) 161-165.

[22] V. Smuleac, D.A. Butterfield, S.K. Sikdar, R.S. Varma, D. Bhattacharyya, Polythiol-functionalized alumina membranes for mercury capture, J. Membr. Sci., 251 (2005) 169-178.

[23] T.F. Baumann, J.G. Reynolds, G.A. Fox, Polymer pendant crown thioethers: synthesis, characterization and Hg2+ extraction studies of polymer-supported thiacrowns ([14]aneS4 and [17]aneS5), React. Funct. Polym., 44 (2000) 111-120.

[24] K.H. Reddy, A.R. Reddy, Removal of heavy metal ions using the chelating polymers derived by the condensation of poly(3-hydroxy-4-acetylphenyl methacrylate) with different diamines, J. Appl. Polym. Sci., 88 (2003) 414-421.

[25] B.F. Senkal, E. Yavuz, Crosslinked poly(glycidyl methacrylate)-based resin for removal of mercury from aqueous solutions, J. Appl. Polym. Sci., 101 (2006) 348-352.

[26] L. Uzun, A. Kara, N. Tuzmen, A. Karabakan, N. Besirli, A. Denizli, Synthesis and characterization of poly(ethylene glycol dimethacrylate-1-vinyl-1,2,4-triazole) copolymer beads for heavy metal removal, J. Appl. Polym. Sci., 102 (2006) 4276-4283.

[27] A.M. Donia, A.A. Atia, K.Z. Elwakeel, Selective separation of mercury(II) using magnetic chitosan resin modified with Schiff's base derived from thiourea and glutaldehyde, J. Hazard. Mater., 151 (2008) 372-379.

[28] W.D. Hand, in, Michigan Technological University, 1982, pp. 114.

[29] D.W. Hand, J.C. Crittenden, W.E. Thacker, User-oriented batch reactor solutions to the homogeneous surface diffusion model, J. Environ. Eng., 109 (1983) 82-101.

[30] Y. Shao, L.F. Molnar, Y. Jung, J. Kussmann, C. Ochsenfeld, S.T. Brown, A.T.B. Gilbert, L.V. Slipchenko, S.V. Levchenko, D.P. O'Neill, R.A. DiStasio Jr., R.C. Lochan, T. Wang, G.J.O. Beran, N.A. Besley, J.M. Herbert, C.Y. Lin, T. Van Voorhis, S.H. Chien, A. Sodt, R.P. Steele, V.A. Rassolov, P.E. Maslen, P.P. Korambath, R.D. Adamson, B. Austin, J. Baker, E.F.C. Byrd, H. Dachsel, R.J. Doerksen, A. Dreuw, B.D. Dunietz, A.D. Dutoi, T.R. Furlani, S.R. Gwaltney, A. Heyden, S. Hirata, C.-P. Hsu, G. Kedziora, R.Z. Khalliulin, P. Klunzinger, A.M. Lee, M.S. Lee, W.Z. Liang, I. Lotan, N. Nair, B. Peters, E. Proynov, I., P.A. Pieniazek, Y.M. Rhee, J. Ritchie, E. Rosta, C.D. Sherrill, A.C. Simmonett, J.E. Subotnik, H.L. Woodcock III, W. Zhang, A.T. Bell, A.K. Chakraborty, D.M. Chipman, F.J. Keil, A. Warshel, W.J. Hehre, H.F. Schaefer, J. Kong, A.I. Krylov, P.M.W. Gill, M. Head-Gordon, Advances in methods and algorithms in a modern quantum chemistry program package, Phys. Chem. Chem. Phys., 8 (2006).

[31] H. Rugner, S. Kleineidam, P. Grathwohl, Long term sorption kinetics of phenanthrene in aquifer materials, Environ. Sci. Technol., 33 (1999) 1645-1651.

[32] E. Yavuz, B.F. Senkal, N. Bicak, Poly(acrylamide) grafts on spherical polyvinyl pyridine resin for removal of mercury from aqueous solutions, React. Funct. Polym., 65 (2005) 121-125.

[33] P.M. Gschwend, S.-C. Wu, Sorption kinetics of hydrophobic organic compounds to natural sediments and soils, Environ. Sci. Technol., 20 (1986) 717-725.

[34] M. Shamsipur, A. Jabbari, M. Esmaeili, Selective transport of mercury as HgCl42− through a bulk liquid membrane using K+-dicyclohexyl-18-crown-6 as carrier, Separ. Purific. Tech., 24 (2001) 139-145.

[35] L.L. Tavlarides, N.K. H., S. Gomez-Salazar, Mercury(II) adsorption from wastewaters using a thiol functional adsorbent, Ind. Eng. Chem. Res., 42 (2003) 1955-1964.

[36] R. Puchta, R. Meier, R. van Eldik, Host-guest complexes of bicyclic hexaamine cryptands – Prediction of ion selectivity by quantum chemical calculations. III, Aust. J. Chem., 60 (2007) 889-897.

[37] R.R. Burnette, J.W. Su, First principles investigation of noncovalent complexation: A [2.2.2]-cryptand ion-ninding selectivity study, Chem. Phys. Chem, 9 (2008) 1989 - 1996.

[38] J. Kim, A.S. Ichimura, R.H. Huang, M.Y. Redko, R.C. Phillips, J.E. Jackson, J.L. Dye, Crystalline salts of Na-and K-(Alkalides) that are stable at room temperature, J. Am. Chem. Soc. , 121 (1999) 10666-10667.

[39] C. Suchentrunk, T. Roßmeier, N. Korber, Crystal structures of the [18]-crown-6 ammoniate C12H24O6·2NH3 and the cryptand [2.2.2] ammoniate C18H36O6N2·2NH3, Kristallorgr., 221 (2006) 162-165.

[40] J.-M. Lehn, F. Montavon, Cryptates. XXV. Stability and selectivity of cation inclusion complexes of polyaza-macrobicyclic ligands. Selective complexation of toxic heavy metal cations, Helv. Chim. Acta, 61 (1978).